JACS
JOURNAL OF THE AMERICAN CHEMICAL SOCIETY
Article
pubs.acs.org/JACS

Thermochemistry of Multiferroic Organic–Inorganic Hybrid Perovskites $[(CH_3)_2NH_2][M(HCOO)_3]$ (M = Mn, Co, Ni, and Zn)

G. P. Nagabhushana, Radha Shivaramaiah, and Alexandra Navrotsky*

Peter A. Rock Thermochemistry Laboratory and NEAT ORU, University of California, Davis, California 95616, United States

Supporting Information

ABSTRACT: Organic–inorganic hybrid materials have enormous potential for applications in catalysis, gas storage, sensors, drug delivery, and energy generation, among others. A class of hybrid materials adopts the ABX_3 perovskite topology. We report here the synthesis and characterization of an isostructural series of dense hybrid perovskites, $[(CH_3)_2NH_2][M(HCOO)_3]$, with M = Mn, Co, Ni, and Zn. These compounds have shown promising multiferroic behavior. Understanding their stability is crucial for their practical application. We report their formation enthalpies based on direct measurement by room-temperature acid solution calorimetry. The enthalpy of formation of this dimethylammonium metal formate series becomes less exothermic in the order Mn, Zn, Co, Ni. The stability of the hybrid perovskite decreases as the tolerance factor increases, unlike trends seen in inorganic perovskites. However, the trends are similar to those seen in a number of ternary transition metal oxides, suggesting that specific bonding interactions rather than geometric factors dominate the energetics.

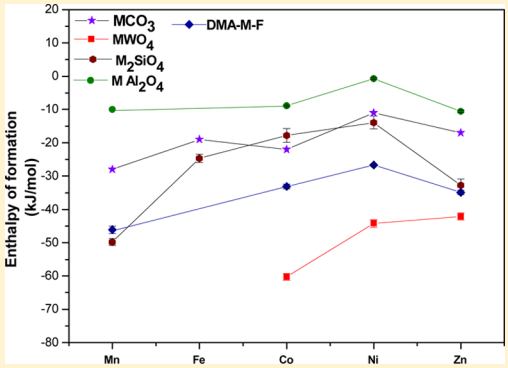

INTRODUCTION

Hybrid organic–inorganic materials have attracted enormous attention in the past decade due to their variety of possible structures and their applications in emerging technologies.[1−3] They can be defined as a homogeneous composite of organic and inorganic components at the molecular level or nanoscale. While the organic moiety offers excellent properties such as structural diversity, elasticity, ease of processing, and efficient luminescence, the inorganic part provides key characteristics such as electrical mobility, thermal stability, band gap engineering, and magnetic and dielectric properties.[4−6] One of the major subclasses of hybrid materials is metal–organic frameworks (MOFs), which can be further divided into two broad categories: nanoporous MOFs and dense MOFs. Currently a majority of the publications in this field describe porous MOFs, which have potential applications in the fields of gas storage and catalysis.[7,8] The structural flexibility and chemical diversity offered by almost unlimited combinations of metal ions and long-chain organic linkers make it possible to design and tailor these materials. Dense hybrid MOF materials are framework structures which incorporate inorganic connectivity in all three crystallographic directions. They are gaining enormous interest because they exhibit a wide range of interesting physical properties, such as superconductivity, colossal magnetoresistance, nonlinear optical effects, electrical conductivity, and luminescence.[9−12] A subset of such hybrid frameworks adopts perovskite-like structures with the general formula ABX_3, where A is a protonated amine, B and a divalent metal, and X is a halide, cyanide, azide, or carboxylate.[13,14] One such example is formate-based perovskites, $[A\text{-}M\text{-}(HCOO)_3]$. They contain a divalent transition metal ion (M^{2+}) which occupies BO_6 octahedra, linked by a formate ($HCOO^-$) bridging ligand to form a cavity which is occupied by an organic cation, as shown in Figure 1. They are gaining significant attention for their ferroelectric and multiferroic properties, which are observed upon cooling due to ordering of amine cations in the perovskite cavity.[15,16]

The organic cation located in the cavity has some degree of motional freedom, a factor that has been exploited to develop

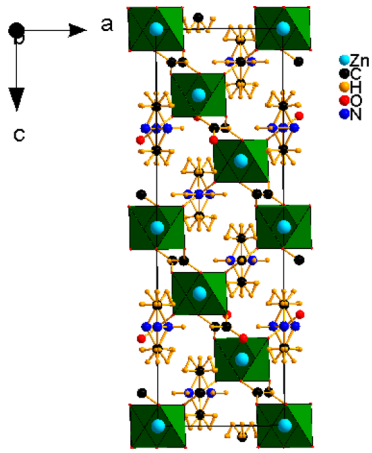

Figure 1. Structure of [DMA-Zn-F] perovskite.

Received: June 12, 2015
Published: July 27, 2015

DOI: 10.1021/jacs.5b06146
J. Am. Chem. Soc. 2015, 137, 10351−10356

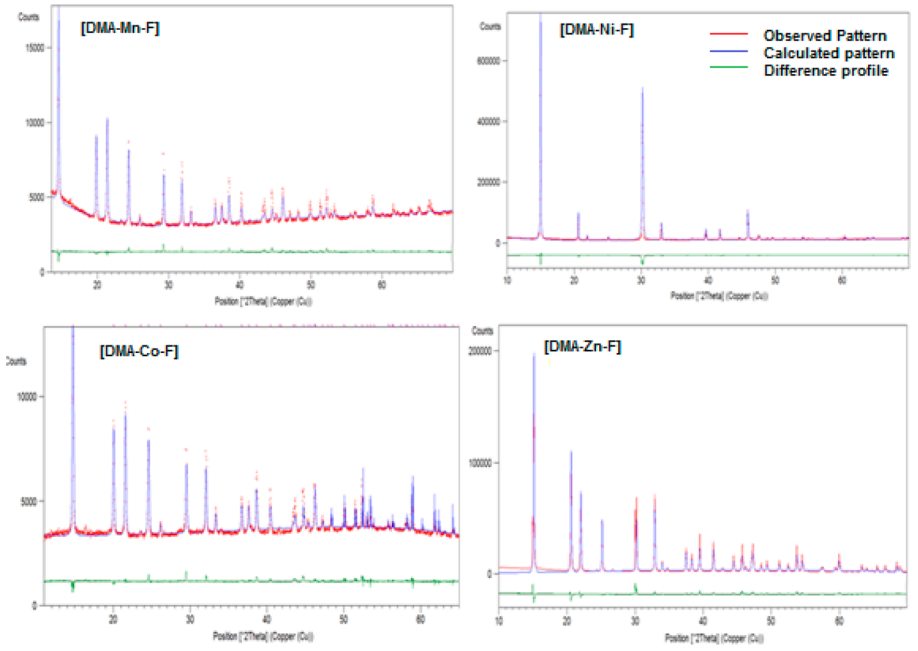

Figure 2. Rietveld fit of PXRD patterns of all four DMA-M-F compounds.

interesting physical properties. At room temperature the "A" site occupied by the alkylammonium cation is disordered, but upon cooling an ordering phase transition occurs, giving a dielectric anomaly at the transition temperature.[17] The ordering of hydrogen bonding (N−H···O) of the alkylammonium cation triggers the ferroelectic ordering at low temperature.[18] Further, the dense hybrid perovskites display large thermal expansion coefficients.[17] The thermal expansion anomaly observed at the phase transition is not related to the elimination or insertion of guest species. Rather, it originates from the order−disorder of the alkylammonium cation inside the cavities and the associated deformations of the $[M(HCOO)_3]^-$ framework, which directly affect the dielectric properties.[19] Likewise, the bridging ligand, namely the formate anion, plays an important role in determining the physical properties. Formate is the simplest carboxylate that can adopt various bridging modes, such as syn−syn, anti−anti, and syn−anti, and it has short bridges to link metal ions and small steric effects.[20,21] The dense MOFs of divalent transition metals are also interesting due to the variation delivered by the magnetic anisotropy and the spin of 3d transition metals.[22,23] One such class of formate hybrid perovskites is dimethylammonium metal formates, $[(CH_3)_2NH_2]M(HCOO)_3]$ (M = Mn, Fe, Co, Ni, and Zn).[21] Each of these compounds with a different metal exhibits a ferroelastic phase transition at a different temperature.[15] Dimethylammonium copper formate was one of the first in this series, reported in 1973.[23] However, its relationship to the hybrid perovskite structure was not recognized until 2005.[24] Since then, there has been growing interest in this class of materials, with a large number of publications dealing with their synthesis, properties, and applications.[25−31] However, there is a lack of understanding of their thermodynamic properties, which raise interesting fundamental questions and are crucial to understanding their synthesis, processing, and stability when they are incorporated into devices. Here we report the synthesis and characterization of dimethylammonium metal formates $[DMA\text{-}M\text{-}(HCOO)_3]$, with M = Mn, Co, Ni, and Zn (hereafter written as [DMA-M-F]), and, for the first time, investigate their thermodynamic properties. We report their formation enthalpies based on direct measurement using room-temperature acid solution calorimetry. We interpret the results in terms of structural factors.

EXPERIMENTAL METHODS

Synthesis. [DMA-M-F] (M = Mn, Co, Ni, and Zn) samples were synthesized by a solvothermal method followed by crystallization. Each sample was synthesized under slightly different conditions. Dimethylammonium manganese formate [DMA-Mn-F] was synthesized as follows. In a typical experiment, 20 mL of *N,N*-dimethylformamide (DMF), 1 mL of ethanol, 1 mL of water, 0.3 mL of formic acid, and 2.1 g of $MnCl_2 \cdot 4H_2O$ were heated for 48 h in a Teflon-lined autoclave at 140 °C.[25] The obtained solution was left to stand at room temperature, and colorless crystals were observed with slow evaporation of water. This process took around 10 days when the solution was left at room temperature. The solid was collected, washed with ethanol, and dried at room temperature. Dimethylammonium nickel formate [DMA-Ni-F] and dimethylammonium cobalt formate [DMA-Co-F] were synthesized under similar solvothermal conditions from the corresponding chlorides with slight changes in the synthetic procedure. A mixture of 5 mmol of $MCl_2 \cdot 6H_2O$, 30 mL of DMF, and 30 mL of deionized water was heated in a Teflon-lined autoclave at 140 °C for 48 h.[32] After slow cooling of the solution to room temperature, the precipitate was removed by filtration. Crystals were obtained by evaporating the supernatant solution at room temperature for about 1 week. The crystals were filtered and washed using ethanol.

Dimethylammonium zinc formate [DMA-Zn-F] crystals were prepared by the hydrolysis of DMF. In a typical synthesis, $Zn(NO_3)_2 \cdot 6H_2O$ (1.73 g) was added to a mixture of DMF (25 mL) and water (7.76 mL). The solution was poured into a Teflon-lined autoclave and heated at 80 °C for 3 days.[25] The solution was left at room temperature for 10 days to get [DMA-Zn-F] crystals, which were washed with ethanol and dried at room temperature.

DMF plays an important role in the syntheses of all these samples. Besides behaving as the source of formate and dimethylammonium ion, DMF also serves as a solvent for the crystallization of [DMA-M-F] crystals, as these compounds are very soluble in H_2O. This is also the reason why the crystal growth takes time, as it involves the evaporation of H_2O, which is a slow process at room temperature.

Characterization. Powder X-ray diffraction (PXRD) of all the samples was measured and recorded using a Bruker-AXS D8 Advance

DOI: 10.1021/jacs.5b06146
J. Am. Chem. Soc. 2015, 137, 10351−10356

diffractometer operated at 40 kV and 40 mA using Cu Kα radiation. Data were collected from 10 to 80° 2θ at a step size of 0.02° 2θ, with 1 s/step. The Rietveld technique was employed for structure refinement of all the phases using X'pert HighScore Plus software. Published crystal structures were used for the data refinement. DIAMOND software was used to visualize the obtained structure and to evaluate bond distances. Thermogravimetric (TG) analysis was performed using a Netzsch 449 TG/DSC instrument under 1 bar Ar atmosphere (25−500 °C, heating rate 5 °C/min, Pt crucible). A Bruker Equinox 55 FTIR spectrometer (range 400−4000 cm^{-1}) operated with Opus software was used to collect IR spectra.

Isothermal Acid Solution Calorimetry. A Calorimetry Sciences Corp. (CSC) 4400 isothermal microcalorimeter operated with IMC data acquisition software was used to measure the enthalpies of dissolution of the samples at 25 °C. Typically, ∼5 mg hand-pressed pellets were dropped into 25 g of 5 M HCl equilibrated in the sample chamber of the calorimeter for about 4 h under mechanical stirring. In the case of anhydrous metal chlorides, which are components of the thermochemical cycle used, pellets were made inside a glovebox operated under N_2 atmosphere. Liquid formic acid, a constituent of the thermochemical cycle, was injected through a Teflon tube that extended into the silica connection tube until approximately 2 cm above the solvent surface. The mass of injected formic acid was determined by weighing the syringe assembly before and after injection. All the weight measurements were done on a Mettler microbalance with an accuracy of 10 μg. The calorimeter was calibrated by dissolving 15 mg pellets of NIST standard reference material KCl in 25 g of water, which corresponds to a reference concentration of 0.008 mol kg^{-1} at 25 °C. The calibration factor was calculated using the known solution enthalpy for the reference concentration of 0.008 mol kg^{-1} and enthalpy of dilution measurements. The total heat effect due to sample dissolution was obtained by integrating the calorimetric signal with a linear baseline in Origin 8.5 software, which was then converted to joules, using the calibration factor obtained using KCl. The enthalpy of formation was calculated using an appropriate thermochemical cycle based on Hess's law (see Table 2). The use of a large amount of 5 M HCl (25 mL) for each calorimetric run eliminates any sample-weight-dependent final state variation in the thermochemical cycle. This methodology is essentially the same as that used in our earlier work on metal−organic frameworks.[33,34]

RESULTS

The PXRD patterns of all the four [DMA-M-F] are shown in Figure 2. Rietveld refinements were performed using the published crystal structures for each of the compounds.[35] All the compounds crystallize in trigonal space group $R\bar{3}$, and the refined lattice parameters are listed in Table 1. In the absence of a structure model for the Co analogue, we use the one for Mn for the refinement of the Co sample.

Table 1. Refined Lattice Parameters of DMA-M-F Samples

sample	space group	a (Å)	c (Å)	R value
[DMA-Mn-F]	$R\bar{3}c$	8.331(2)	22.888(4)	15.1
[DMA-Zn-F]	$R\bar{3}c$	8.204(1)	22.295(3)	6.8
[DMA-Co-F]	$R\bar{3}c$	8.317(1)	22.850(6)	8.1
[DMA-Ni-F]	$R\bar{3}c$	8.138(3)	21.952(8)	7.1

The a parameter with different M varies according to ionic radii of the divalent cation in the order Ni < Zn < Co < Mn. All the four hybrid perovskites are isostructural. The crystal structure obtained after refinement of [DMA-Zn-F] as a representative is shown in Figure 1. A part of this unit cell is shown in Figure 3. It consists of a slightly enlarged NaCl type framework of $[M(HCOO)^-_3]$ with the dimethylammonium cation occupying the cavities showing a trigonal disorder as

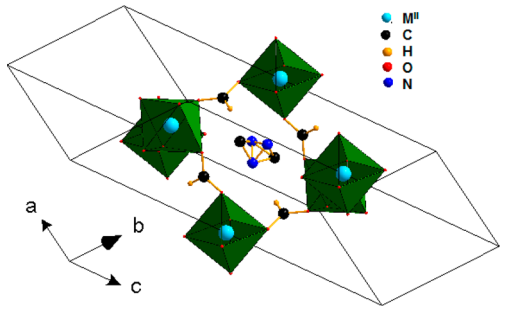

Figure 3. Part of the unit cell of [DMA-M-F] showing metal atoms octahedrally coordinated with bridging formate and dimethylammonium cation in the cavity.

described earlier.[19] Each metal ion is connected to its six nearest neighbors through six formate bridges as shown in Figure 3. The M−O distance for Mn is 2.187 Å, Co is 2.109 Å, and Ni is 2.095 Å, which follows the order of their ionic radii. However, the Zn−O bond distance is 2.116 Å. The obtained atomic parameters are given in Table S1.

TG curves of all the samples are shown in Figure 4a. [DMA-Mn-F], [DMA-Co-F], and [DMA-Zn-F] show two-step mass loss between 150 and 350 °C. The first loss occurs at ∼150−200 °C, which corresponds to the loss of one amine and one formic acid per formula unit of compound, leading to the formation of a metal formate $[M(HCOO)_2]$. The observed experimental percentage weight loss and calculated stoichiometric values (in parentheses) are 39.98% (38.6), 37.16% (37.58), and 38.88% (38.01) for [DMA-Mn-F], [DMA-Co-F], and [DMA-Zn-F], respectively. In the second step observed at ∼250 °C, there is a mass loss of about 30% due to decomposition of metal formate leading to the formation of the binary oxide. However, in [DMA-Ni-F], mass loss occurs in one step instead of two, from ∼150 to 250 °C, indicating that the decomposition of dimethylammonium and formate occurs simultaneously. The total observed mass loss of 67.22% (68.71) corresponds to the loss of one amine and three formate per formula unit of [DMA-Ni-F].

The FTIR spectra are shown in Figure 4b. The observed vibrational modes of all four compounds are similar. The bands observed are characteristic of the protonated amine cation and $HCOO^-$ and can be subdivided into internal vibrations of the dimethylammonium cation and formate ions and the lattice vibrations. The symmetric O−C−O stretching and bending modes of formate appear at ∼1350 and ∼795 cm^{-1}, respectively. The symmetric stretching modes of $(-CH_2-)$ of dimethylammonium cation appears at ∼1458 cm^{-1}, and the $(-NH_2-)$ asymmetric stretching modes appears at ∼1630 cm^{-1}.[35]

Isothermal Acid Solution Calorimetry. The enthalpies of formation of the [DMA-M-F] were calculated using the thermochemical cycle shown in Table 2.

The measured drop solution enthalpies (ΔH_{ds}) of all four [DMA-M-F] samples and the constituents of thermochemical cycle used to calculate formation enthalpies are listed in Table 3. The formation enthalpy values of all the [DMA-M-F] crystals calculated from their corresponding metal chlorides are exothermic. The enthalpies of formation of [DMA-Mn-F], [DMA-Co-F], [DMA-Ni-F], and [DMA-Zn-F] are −47.95 ± 1.12, −34.89 ± 0.68, −28.45 ± 0.25, and −41.66 ± 0.66 kJ/mol, respectively.

DOI: 10.1021/jacs.5b06146
J. Am. Chem. Soc. 2015, 137, 10351−10356

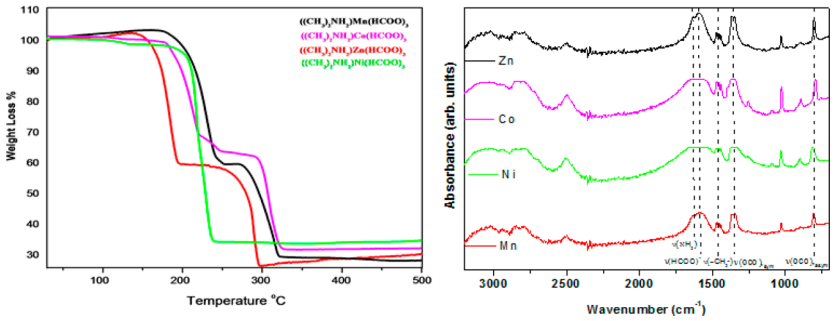

Figure 4. (a) TG and (b) FTIR spectra of all four [DMA-M-F] samples.

Table 2. Thermochemical Cycle Used To Calculate the Formation Enthalpy of [DMA-M-F] (M = Mn, Co, Zn, and Ni)[a]

$M^{2+}_{(aq)} + [(CH_3)_2NH_2]^+_{(aq)} + 3HCOO^-_{(aq)} \rightarrow [(CH_3)_2NH_2]M(HCOO)_{3(s)}$	$-\Delta H_1$
$MCl_{2(s)} + 2H^+_{(aq)} \rightarrow M^{2+}_{(aq)} + 2HCl_{(5M\ HCl,aq)}$	ΔH_2
$[(CH_3)_2NH]\cdot HCl_{(s)} + H^+_{(aq)} \rightarrow [(CH_3)_2NH_2]^+_{(aq)} + HCl_{(5M\ HCl,aq)}$	ΔH_3
$3[HCOOH\cdot xH_2O_{(l)} \rightarrow 3HCOO^-_{(aq)} + 3H^+_{(aq)} + 3xH_2O_{(aq)}]$	$3\Delta H_4$
$3[xH_2O_{(l)} \rightarrow xH_2O_{(aq)}]$	$3\Delta H_5$
$MCl_{2(s)} + [(CH_3)_2NH].HCl_{(s)} + 3HCOOH\cdot xH_2O_{(l)} \rightarrow [(CH_3)_2NH_2]M(HCOO)_{3(s)} + 3\cdot xH_2O_{(l)} + 3HCl_{(aq)}$	ΔH_6

$$\Delta H_{6(f,298)} = -\Delta H_1 + \Delta H_2 + \Delta H_3 + 3\Delta H_4 + 3\Delta H_5$$

[a]M = Mn, Co, Ni, and Zn; x = 0.07670 H_2O per formula unit.

Table 3. Thermochemical Data Used for the Calculation of Enthalpy of Formation of [DMA-M-F] (M = Mn, Co, Zn, and Ni)

compound	ΔH_{ds} (kJ/mol)[a]	ΔH_f (kJ/mol)
DMA·HCl	−2.78 ± 0.39 (4)	
HCOOH	−0.84 ± 0.17 (4)	
H_2O	−0.5[b]	
$MnCl_2$	−48.06 ± 1.01(4)	
$CoCl_2$	−33.80 ± 0.49 (4)	
$NiCl_2$	−27.04 ± 0.91 (3)	
$ZnCl_2$	−44.52 ± 0.86(4)	
[DMA-Mn-F]	−5.29 ± 0.06 (4)	−47.95 ± 1.12
[DMA-Co-F]	−4.09 ± 1.34(4)	−34.89 ± 0.68
[DMA-Ni-F]	−3.77 ± 0.83(4)	−28.45 ± 0.25
[DMA-Zn-F]	−8.04 ± 0.37(4)	−41.66 ± 0.66

[a]Values given in parentheses are the number of experiments performed. [b]References 33 and 36.

DISCUSSION

Formation enthalpies of inorganic oxide perovskites are often correlated with tolerance factor,[37,38] which is an indicator of distortion resulting from A−O and B−O bond length misfit. It is given by

$$t = (r_A + r_O)/\sqrt{2}(r_B + r_O) \quad (1)$$

where r_A and r_B are the ionic radii of the cations which occupy the A and B sites and r_O is the ionic radius of the oxygen anion.[39] However, among hybrid perovskites the concept of tolerance factor is less explored except for a recent report by Cheetham et al.[40] We calculate the tolerance factor for the compounds studied in the present work based on their approach and try to correlate the values to enthalpy of formation obtained by calorimetry.

In hybrid perovskites we are dealing with molecular cations, where varying bond length due to hydrogen bonding interactions make it difficult to define an ionic radius. To overcome this difficulty, Cheetham et al. used the crystallographic data of known perovskite-like hybrid frameworks and estimated a consistent set of effective radii for different organic ions.[40,41] However, they applied a rigid sphere model for organic cations and assumed rotational freedom. We have used their equation to calculate the tolerance factor for the present set of compounds,

$$t = (r_{A,eff} + r_{X,eff})/\sqrt{2}(r_B + 0.5h_{X,eff}) \quad (2)$$

The effective cation radius is given by

$$r_{A,eff} = r_{mass} + r_{ion} \quad (3)$$

where r_{mass} is the distance between the center of mass of the molecule and the atom with the largest distance to the center of mass, excluding hydrogen atoms, and r_{ion} is the corresponding ionic radius. For dimethylammonium r_{mass} = 126 pm (distance between center of mass of dimethylammonium and O atom of formate anion), r_{ion} = 146 pm (ionic radius of oxygen), and the calculated $r_{A,eff}$ = 272 pm. The anions are treated as rigid cylinders because of their high anisotropy. For formate r_{Xeff} = 136 pm, and $h_{X,eff}$ = 447 pm.

Tolerance factors calculated using eq 2 for [DMA-M-F] hybrid perovskites (M = Mn, Co, Ni, and Zn) are shown in Table 4. Since formate is a weak field ligand, high spin radii of

DOI: 10.1021/jacs.5b06146
J. Am. Chem. Soc. 2015, 137, 10351−10356

Table 4. Calculated Tolerance Factors of [DMA-M-F] Hybrid Perovskites and Their Formation Enthalpies

[DMA-M-F]	enthalpy of formation (kJ/mol)	tolerance factor	cation radius[a] (pm)
[DMA-Mn-F]	−47.95 ± 1.12	0.941	83
[DMA-Co-F]	−34.89 ± 0.68	0.968	74.5
[DMA-Ni-F]	−28.45 ± 0.25	0.986	69
[DMA-Zn-F]	−41.66 ± 0.66	0.970	74

[a]Reference 42.

transition metal ions are used for the calculation. With "A" (DMA) and "X" ($HCOO^-$) being the same for all the four compounds and "M" being variable, the calculated tolerance factor for Ni is highest and that for Mn lowest.

The correlation between the enthalpy of formation of the four isostructural [DMA-M-F] compounds and the calculated

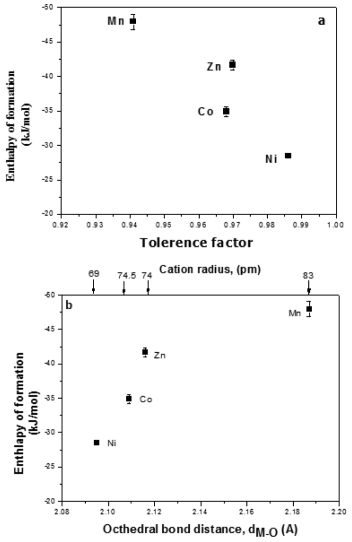

Figure 5. Enthalpy of formation of [DMA-M-F] (M = Mn, Co, Zn, and Ni) (a) as a function of the tolerance factor and (b) as a function of the M−O octahedral bond distance.

tolerance factor is shown in Figure 5a. In inorganic oxide perovskites, ideal cubic structures form when tolerance factor is close to 1, and distorted perovskite structures are generally observed for materials with a tolerance factor in the range of 0.8−0.95.[37] The stability of such inorganic structures increases as the tolerance factor approaches unity.[43,44] Applying similar concepts to the present work where all four hybrid frameworks exhibit a tolerance factor between 0.941 and 0.986, we predict that these materials would form with favorable energetics, which is indeed observed in our calorimetric measurements. However, these perovskites show lower symmetry than expected from their tolerance factors, which is presumably related to the presence of organic ligands.

Furthermore, the trend in formation enthalpy vs tolerance factor (see Figure 5a) is opposite from that of inorganic perovskites, where the enthalpy of formation becomes more exothermic with increasing tolerance factor,[45,46] although oxide perovskites with divalent transition metals are not available for comparison. ABF_3 fluoride perovskites with divalent transition metal ions do exist,[47,48] but there is a lack of sufficient thermodynamic data to compare the stabilities of fluoride perovskites with their formate counterparts.[49,50]

The above observations thus suggest that geometric mismatch as measured by tolerance factor is not a major driver of thermodynamic stability in these hybrid perovskites. Furthermore, unlike in the oxide perovskites, there are no direct M-O-M linkages in the hybrid formate perovskites, and the two metal atoms are linked through a bridging formate ligand by M-O-C-O-M linkages. Figure 5b shows the enthalpy of formation as a function of M−O bond distance obtained by structure refinement of the PXRD patterns. [DMA-Ni-F] with the smallest M−O bond distance has the lowest energetic stability, and [DMA-Mn-F] with the largest M−O bond distance is the most stable in the series. On the other hand, the enthalpy of formation becomes more negative with increasing cation radius in the B site. This may be because with increase in the size of the transition metal cation its basicity increases as well.

In the absence of sufficient thermochemical data for Formate-perovskites with divalent transition metal cations and because there are no oxide perovskites with divalent transition metals in B sites, we used thermochemical data of other ternary oxides containing divalent transition metals[51−56] to compare observed energetic trends (Figure 6).

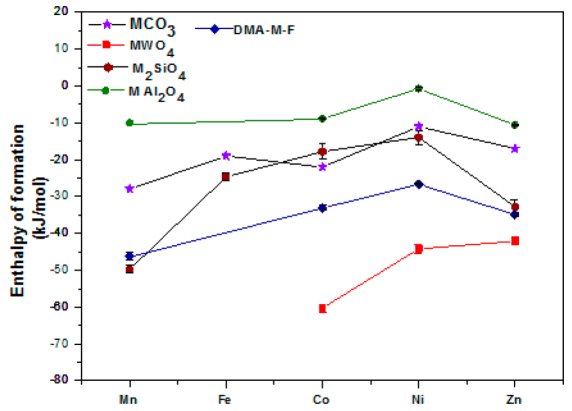

Figure 6. Enthalpy of formation of ternary oxides containing divalent transition metals compared with [DMA-M-F].

Figure 6 shows that enthalpy of formation of all these ternary oxides from the binary oxides is most exothermic for manganese and becomes gradually less exothermic for iron, cobalt, and nickel. Overall the zinc compounds are comparable in enthalpy or slightly more stable than those of iron, cobalt, and nickel. Differences in zinc coordination (octahedral vs tetrahedral) may play a role in these variations. The trend for the [DMA-M-F] hybrid perovskites with M = Mn, Co, Ni, and Zn is similar to trends in these inorganic materials. Furthermore, the enthalpy of formation of the ternary inorganic transition metal materials becomes less exothermic with decreasing acidity of the other oxide (acidity decreases in the order CO_2, WO_3, SiO_2, Al_2O_3). The hybrid perovskites fall between the tungstates and silicates in Figure 6, suggesting that the formate anion in these perovskites is intermediate in acidity between tungstate and silicate.

CONCLUSIONS

This study of the enthalpies of formation of dense MOFs with a perovskite structure, [DMA-M-F], shows that they have stabilities comparable to those of a number of inorganic ternary oxides. Among the four isostructural compounds we

DOI: 10.1021/jacs.5b06146
J. Am. Chem. Soc. 2015, 137, 10351−10356

studied, the Mn analogue is most stable, followed by Zn, Co, and Ni. The energetics of these ternary transition metal materials seem to be governed more by the acid−base properties of the oxide of the associated moiety and the transition metal, respectively, than by bond length misfit as measured by the tolerance factor.

■ ASSOCIATED CONTENT

Supporting Information

The Supporting Information is available free of charge on the ACS Publications website at DOI: 10.1021/jacs.5b06146.

Crystallographic data obtained from Rietveld refinements of [DMA-Mn-F], [DMA-Zn-F], and [DMA-Ni-F], Tables S1−S3 (PDF)

■ AUTHOR INFORMATION

Corresponding Author

*anavrotsky@ucdavis.edu

Notes

The authors declare no competing financial interest.

■ ACKNOWLEDGMENTS

This work was supported by the U.S. Department of Energy, grant DEFG0203ER46053.

■ REFERENCES

(1) Mitzi, D. B. *J. Chem. Soc., Dalton Trans.* **2001**, *1*, 1.
(2) Mitzi, D. B.; Feild, C. A.; Harrison, W. T. A.; Guloy, A. M. *Nature (London, U. K.)* **1994**, *369*, 467.
(3) Mitzi, D. B.; Wang, S.; Feild, C. A.; Chess, C. A.; Guloy, A. M. *Science* **1995**, *267*, 1473.
(4) Férey, G. *Chem. Soc. Rev.* **2008**, *37*, 191.
(5) Cheetham, A. K.; Rao, C. N. R. *Science* **2007**, *318*, 58.
(6) Kitagawa, S.; Kitaura, R.; Noro, S. *Angew. Chem., Int. Ed.* **2004**, *43*, 2334.
(7) Morris, R. E.; Wheatley, P. S. *Angew. Chem., Int. Ed.* **2008**, *47*, 4966.
(8) Lee, J.; Farha, O. K.; Roberts, J.; Scheidt, K. A.; Nguyen, S. T.; Hupp, J. T. *Chem. Soc. Rev.* **2009**, *38*, 1450.
(9) Kurmoo, M. *Chem. Soc. Rev.* **2009**, *38*, 1353.
(10) Allendorf, M. D.; Bauer, C. A.; Bhakta, R. K.; Houk, R. J. T. *Chem. Soc. Rev.* **2009**, *38*, 1330.
(11) Stroppa, A.; Jain, P.; Barone, P.; Marsman, M.; Perez-Mato, J. M.; Cheetham, A. K.; Kroto, H. W.; Picozzi, S. *Angew. Chem., Int. Ed.* **2011**, *50*, 5847.
(12) Bogani, L.; Wernsdorfer, W. *Nat. Mater.* **2008**, *7*, 179.
(13) Horiuchi, S.; Tokura, Y. *Nat. Mater.* **2008**, *7*, 357.
(14) Besara, T.; Jain, P.; Dalal, N. S.; Kuhns, P. L.; Reyes, A. P.; Kroto, H. W.; Cheetham, A. K. *Proc. Natl. Acad. Sci. U. S. A.* **2011**, *108*, 6828.
(15) Di Sante, D.; Stroppa, S.; Jain, P.; Picozzi, S. *J. Am. Chem. Soc.* **2013**, *135*, 18126.
(16) Wang, Z.; Hu, K.; Gao, S.; Kobayashi, H. *Adv. Mater.* **2010**, *22*, 1526.
(17) Sánchez-Andújar, M.; Presedo, S.; Yáñez-Vilar, S.; Castro-García, S.; Shamir, J.; Señarís-Rodríguez, M. A. *Inorg. Chem.* **2010**, *49*, 1510.
(18) (a) Tian, Y.; Stroppa, A.; Chai, Y.; Yan, L.; Wang, S.; Barone, P.; Picozzi, S.; Sun, Y. *Sci. Rep.* **2014**, *4*, 6062. (b) Fu, D. W.; Zhang, W.; Cai, H. L.; Zhang, Y.; Ge, J. Z.; Xiong, R. G.; Huang, S. D.; Nakamura, T. *Angew. Chem., Int. Ed.* **2011**, *50*, 11947−11951. (c) Wang, W.; Yan, L. Q.; Cong, J.-Z.; Zhao, Y.-L.; Wang, F.; Shen, S.-P.; Zou, T.; Zhang, D.; Wang, S.-G.; Han, X.-F.; Sun, Y. *Sci. Rep.* **2013**, *3*, 2024.
(19) Thomson, R. I.; Jain, P.; Cheetham, A. K.; Carpenter, M. A. *Phys. Rev. B: Condens. Matter Mater. Phys.* **2012**, *86*, 214304.
(20) Magalhaes, A. L.; Madail, S. R. R. S.; Ramos, M. J. *Theor. Chem. Acc.* **2000**, *105*, 68.
(21) Wang, Z.; Zhang, B.; Inoue, K.; Fujiwara, H.; Otsuka, T.; Kobayashi, H.; Kurmoo, M. *Inorg. Chem.* **2007**, *46*, 437.
(22) Wang, K. F.; Liu, J. M.; Ren, Z. F. *Adv. Phys.* **2009**, *58*, 321.
(23) Sletten, E.; Jensen, L. H. *Acta Crystallogr., Sect. B: Struct. Crystallogr. Cryst. Chem.* **1973**, *29*, 1752.
(24) Jain, P.; Ramachandran, V.; Clark, R. J.; Zhou, H. D.; Toby, B. H.; Dalal, N. S.; Kroto, H. W.; Cheetham, A. K. *J. Am. Chem. Soc.* **2009**, *131*, 13625.
(25) Jain, P.; Dalal, N. S.; Toby, B. H.; Kroto, H. W.; Cheetham, A. K. *J. Am. Chem. Soc.* **2008**, *130*, 10450.
(26) Hu, K.-L.; Kurmoo, M.; Wang; Gao, M. S. *Chem. - Eur. J.* **2009**, *15*, 12050.
(27) Ramesh, R. *Nature* **2009**, *461*, 1218.
(28) Rao, C. N. R.; Cheetham, A. K.; Thirumurugan, A. *J. Phys.: Condens. Matter* **2008**, *20*, 083202.
(29) Sanchez-Andujar, M.; Presedo, S.; Yanez-Vilar, S.; Castro-Garcıa, S.; Shamir, J.; Senarıs-Rodrıguez, M. A. *Inorg. Chem.* **2010**, *49*, 1510.
(30) Spaldin, N. A.; Cheong, S. W.; Ramesh, R. *Phys. Today* **2010**, *63*, 38.
(31) Clausen, H. F.; Poulsen, R. D.; Bond, A. D.; Chevallier, M. A. S.; Iversen, B. B. *J. Solid State Chem.* **2005**, *178*, 3342.
(32) Wang, X. Y.; Gan, L.; Zhang, S. W.; Gao, S. *Inorg. Chem.* **2004**, *43*, 4615.
(33) Hughes, J. T.; Navrotsky, A. *J. Am. Chem. Soc.* **2011**, *133*, 9184.
(34) Hughes, J. T.; Navrotsky, A. *J. Chem. Thermodyn.* **2011**, *43*, 980.
(35) (a) Maczka, M.; Gagor, A.; Macalik, B.; Pikul, A.; Ptak, M.; Hanuza, J. *Inorg. Chem.* **2014**, *53*, 457−467. (b) Mączka, M.; Ptak, M.; Macalik, L. *Vib. Spectrosc.* **2014**, *71*, 98−104.
(36) Parker, V. B. *Thermal Properties of Aqueous Uni-univalent Electrolytes*; National Bureau of Standards: Washington, DC, April 1965.
(37) Navrotsky, A. *AIP Conf. Proc.* **2000**, *535*, 288.
(38) Navrotsky, A. *J. Mater. Chem.* **2010**, *20*, 10577.
(39) Goldschmidt, V. M. *Naturwissenschaften* **1926**, *14*, 477.
(40) Kieslich, G.; Sun, S.; Cheetham, A. K. *Chem, Sci.* **2014**, *5*, 4712.
(41) Kieslich, G.; Sun, S.; Cheetham, A. K. *Chem, Sci.* **2015**, *6*, 3430.
(42) Shannon, R. D. *Acta Crystallogr., Sect. A: Cryst. Phys., Diffr., Theor. Gen. Crystallogr.* **1976**, *32*, 751.
(43) Navrotsky, A. *ECS Trans.* **2012**, *45*, 11.
(44) Navrotsky, A. *Pure Appl. Chem.* **1994**, *66*, 1759.
(45) Yokokawa, H.; Sakai, N.; Kawada, T.; Dokiya, M. *Solid State Ionics* **1992**, *52*, 43.
(46) Yokokawa, H.; Sakai, N.; Kawada, T.; Dokiya, M. *J. Electrochem. Soc.* **1991**, *138*, 2719.
(47) Watson, G. W.; Parker, S. C.; Wall, A. *J. Phys.: Condens. Matter* **1992**, *4*, 2097.
(48) Dobson, D. P.; Hunt, S. A.; Lindsay-scott, A.; Wood, I. G. *Phys. Earth Planet. Inter.* **2011**, *189*, 171.
(49) Seddik, T.; Khenata, R.; Merabiha, O.; Bouhemadou, A.; Bin-Omran, S.; Rached, D. *Appl. Phys. A: Mater. Sci. Process.* **2012**, *106*, 645.
(50) Topor, L.; Navrotsky, A.; Zhao, Y.; Weidner, D. J. *J. Solid State Chem.* **1997**, *132*, 131.
(51) Navrotsky, A.; Kleppa, O. J. *Inorg. Chem.* **1969**, *8*, 756.
(52) Navrotsky, A. *J. Inorg. Nucl. Chem.* **1971**, *33*, 4035.
(53) Navrotsky, A.; Kleppa, O. J. *J. Inorg. Nucl. Chem.* **1968**, *30*, 479.
(54) Navrotsky, A. *Chem. Mater.* **1998**, *10*, 2787.
(55) Navrotsky, A. *Prog. Solid State Chem.* **1976**, *11*, 203.
(56) Navrotsky, A. *Prog. Solid State Chem.* **1987**, *17*, 53.

■ NOTE ADDED AFTER ASAP PUBLICATION

Due to a production error, the first column of Tables 3 and 4 published in error on August 6, 2015. The corrected version published August 7, 2015.

DOI: 10.1021/jacs.5b06146
J. Am. Chem. Soc. 2015, 137, 10351−10356